RESEARCH PAPER

PCCP
www.rsc.org/pccp

Pd L_3 edge XANES investigation of the electronic and geometric structure of Pd/Ag–H membranes

Laurens C. Witjens, J. H. Bitter, A. J. van Dillen, K. P. de Jong and F. M. F. de Groot*

Inorganic Chemistry and Catalysis, Debye Institute, Utrecht University, P.O. Box 80083, Utrecht 3508 TB, the Netherlands. E-mail: f.m.f.degroot@chem.uu.nl; Fax: +31 30 2511027; Tel: +31 30 2536763

Received 11th February 2004, Accepted 19th May 2004
First published as an Advance Article on the web 26th May 2004

The electronic and geometric structure of the Pd/Ag–H system, an important hydrogen membrane structure, has been studied with x-ray absorption spectroscopy. Palladium L_3 XANES measurements in both vacuum and *in situ* under hydrogen atmosphere were performed at room temperature on an ideally mixed $Pd_{0.8}Ag_{0.2}$ system obtained with bi-sputtering, and on a pure Pd system obtained with electroless plating. A model of fcc-Pd/Ag with the Ag atoms evenly distributed through the system and the hydrogen atoms placed in the octahedral holes was able to explain the observed XANES in great detail. FEFF calculations show that the Pd/Ag–H system generates an anti-bonding Pd–H band, in close agreement with the experimental results. In addition the calculations show that the hydrogen content of the system strongly influences the XANES, especially the intensity of the white-line and the anti-bonding peak. In contrast the influence of the Ag atoms is limited to relatively small changes in the white-line intensity. However change of the Ag distribution within the Pd/Ag fcc lattice from well-mixed to clustered was found to have a significant influence on the Pd L_3 edge white-line intensity.

1. Introduction

Thin $Pd_{0.77}Ag_{0.23}$ films on inert, porous supports such as α-alumina, Vycor glass or porous stainless steel are very important membrane materials.[1–4] Applications vary from separating H_2 from gas streams to use in a membrane reactor in hydrogenation or dehydrogenation reactions.[3,5–7]

Hydrogen permeates through solid metals *via* the solution–diffusion mechanism;[3] hydrogen is dissociatively chemisorbed on the surface of the metal, absorbed into the bulk metal as atoms and diffuses through the metal to recombine at and desorb from the opposite surface. Within the bulk of both Pd and Pd/Ag alloys the hydrogen atoms prefer to be located in the octahedral interstices of the face-centered cubic (fcc) lattice,[3,8] most likely travelling from one octahedral site to the next *via* a tetrahedral site.[3,9]

It is well documented[1,10,11] that the optimal Pd/Ag membrane composition, based on both maximum hydrogen permeability and lifetime considerations, is 23 at% Ag. The lifetime of pure Pd membranes is largely limited by the so-called hydrogen embrittlement. This phenomenon is caused by transition between two different palladium hydride phases (α and β) and induces strong local tensions in the metal film resulting in microcracking and finally mechanical failure. Alloying Pd with 23 at% Ag lowers the critical temperature, $T_c(\alpha,\beta)$, for the coexistence of the α and β phases so that only a single Pd/Ag–H phase is formed above ambient temperature[3,11,12] and hydrogen embrittlement is prevented.

The Pd–H system has been investigated extensively in the past, including studies on the electronic structure with X-ray absorption.[13,14] Pd/Ag alloys have also received ample attention.[15,17] Despite its important applications in the hydrogen purification field the Pd/Ag–H system has been largely neglected. Only recently some papers[9,18] have been published on this subject, however these articles are purely theoretical works. One of the findings of our experimental work, as was shown with some prelimenary results at the XAFS-12 meeting in Malmö,[19] is the deviation of the Pd L_3 edge XANES of the Pd/Ag–H system from the expectations raised by the Pd–H and Pd/Ag XANES. Differences in the local geometry of Pd–H and Pd/Ag–H are a likely cause of the observed changes. Clarification of this phenomenon could be a major step for improving membrane performance.

In this full paper the experimental XANES results are analyzed in detail and modelled with the FEFF 8.2 program,[20] an *ab initio* self-consistent real space multiple-scattering code for simultaneous calculations of x-ray absorption spectra and the electronic structure, to determine the origin of the electronic structure of the Pd/Ag–H system. For the modelling work fcc crystal structures were used and it was assumed that the hydrogen atoms occupy the octahedral holes both in pure Pd and in Pd/Ag alloys. Although there is a small barrier[9] of 81.4 meV $atom^{-1}$ between octahedral and tetrahedral hole occupation, Boltzmann's distribution law states that at ambient temperature only 4% of the hydrogen atoms will be located in the tetrahedral holes.

It was investigated whether such models could satisfactorily explain the observed Pd/Ag–H Pd L_3 edge XANES or whether significant changes to the structure were needed. Secondly, the influence of the Ag distribution within the Pd/Ag fcc lattice on the XANES was considered, since the Ag distribution is of major importance to the membrane performance. If locally areas are enriched or impoverished in Ag the hydrogen permeability in those areas, and as a consequence the overall hydrogen permeability, will be decreased. Furthermore it is likely that Ag poor areas can act as crystallization points where hydrogen embrittlement and subsequent microcracking can occur, potentially resulting in mechanical failure. Inadequate mixing is therefore expected to seriously limit the performance and lifetime of the membranes. Therefore calculations were not only performed on systems with homogeneously distributed Ag atoms, but also on a system with all Ag atoms concentrated in one cluster.

2. Materials and methods

A 3–4 μm thick Pd film deposited on an α-alumina tube with the electroless plating method,[1,5] was obtained from ECN

DOI: 10.1039/b402540g

(Petten, the Netherlands). A cross-section of the sample was studied with SEM.

A 750 nm $Pd_{0.8}Ag_{0.2}$ sample on a SiO_2/Si wafer (with 25 nm Ti adhesion layer) obtained with bi-sputtering was received from the MESA$^+$ institute of the University Twente (Enschede, the Netherlands). The surface of the sample was studied with SEM. XPS depth-profiling of this sample was performed in our laboratory to check the homogeneity of the Ag distribution. XPS measurements were alternated with sputtering with an Ar^+ ion beam until the support material was detected. The XPS data were obtained with a Vacuum Generators XPS system, using a CLAM-2 hemispherical analyser for electron detection. Non-monochromatic Al(K_α) X-ray radiation was used for exciting the photo electron spectra using an anode current of 20 mA at 10 keV. The pass energy of the analyser was set at 50 eV. The survey scan was taken with a pass energy of 100 eV.

At the E4 beamline of the HASYLAB facility (Hamburg, Germany) the Pd L_3-edge XANES of the pure Pd and Pd/Ag alloy samples were determined in vacuum and under a H_2 atmosphere of 1.5 bar. The measurements were performed at ambient temperature using a Ge single channel fluorescence detector with a diameter of 2.5 cm. At least two scans were averaged for each measurement. The pre-edges and backgrounds were subtracted and the measurements were normalised at 50 eV beyond the edge. Some saturation effects due to self-absorption were visible when comparing our fluorescence results to transmission results from Coulthard and Sham.[16] A numerical correction was determined based on the vacuum measurements of the two samples and applied to the hydrogen measurements. The correction was based on work by Schroeder;[21] for a 90° scattering angle the intensity of the fluorescence yield (I_F) is given as a function of the absorption cross section (μ_x) and the background absorption (μ_B):

$$I_F \approx \frac{\mu_x}{\mu_x + \mu_B} \quad (1)$$

The value of μ_B was determined by steering the relative intensity of the white-line (compared to the baseline) to the values for pure Pd respectively $Pd_{0.8}Ag_{0.2}$ as determined by Coulthard and Sham,[16] while the baseline was kept at 1 with the aid of a normalization factor. The energy scales of the spectra were calibrated on the point of inflection of the Pd L_3 edge, 3173.3 eV,[22] of the pure Pd sample in vacuum. During the course of the experiments the energy scale shifted 0.3 eV.

FEFF 8.2 calculations[20] were performed with clusters of 121 or 139 atoms. The clusters were centered round a single Pd atom, the FEFF target. First a model was created for the Pd–H system, in the second step this model was applied to the Pd/Ag–H system and finally the hydrogen content of the model was optimized and the influence of the Ag distribution on the XANES was studied. The models were based on the fcc lattice structure with the Pd and Ag atoms placed in the fcc locations and the hydrogen atoms evenly distributed over the octahedral holes. Similarly the Ag atoms were evenly distributed over the fcc positions in the Pd/Ag models, except for the Pd/Ag H_2 cluster model. In this case all Ag atoms were clustered within one unit cell (Fig. 1), to determine the effect of the Ag distribution on the XANES.

The lattice constant was set to 4.025 Å for all models (Pd and Pd/Ag), as found for $PdH_{0.6}$,[23] based on the strong influence of the hydrogen atoms on the lattice constant compared to the relative weak effect of alloying Pd with 20 at% Ag. The lattice constant only increases from 3.894 Å[23] for pure Pd to 3.924 Å for $Pd_{0.8}Ag_{0.2}$,† while introducing 0.6 H into pure Pd increases the lattice constant to 4.025 Å. Maintaining the same lattice constant for all models was a reasonable assumption and facilitated the comparison of the models. All models had five metal shells and five hydrogen shells. In Table 1 the characteristics of the models are listed.

† A linear relation between the lattice constant and the Ag content (Vegard's law) was derived for Pd/Ag alloys from XRD lattice constant data[33,34] and was used to determine this lattice constant.

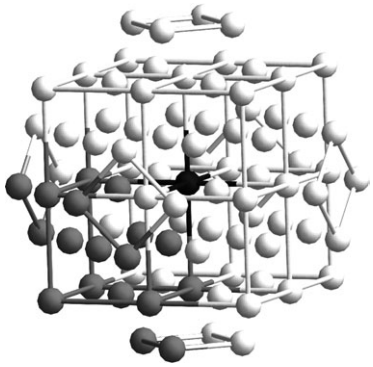

Fig. 1 The $Pd_{0.8}Ag_{0.2}H_{0.4}$ cluster (model #4) minus the hydrogen atoms; note the central Pd atom and FEFF target (black sphere), the other Pd atoms (white spheres) and the Ag cluster (grey spheres).

Table 1 Characteristics of the FEFF 8.2 models

			Number of atoms in model		
Model (#)	Description	Ag distribution	Pd	Ag	H
1	$PdH_{0.6}$	—	87	—	52
2	$Pd_{0.8}Ag_{0.2}H_{0.6}$	Random	69	18	52
3	$Pd_{0.8}Ag_{0.2}H_{0.4}$	Random	69	18	34
4	$Pd_{0.8}Ag_{0.2}H_{0.4}$	Clustered	69	18	34

For all FEFF 8.2 calculations the core hole parameter has been included.[24] The SCF parameter was set to 4.1 Å, which corresponds to two metal and two hydrogen shells. The FMS parameter was set to 7.0 Å and includes the complete models as given in Table 1. Corrections of the Fermi level were necessary to compensate for the value determined by the FEFF 8.2 code. The size of the correction was determined by matching the intensity of the white-line absorption of the FEFF calculations with the experimental results. For all models a correction of 2.2 eV was used.

3. Results and discussion

3.1 Sample characterisation

Inspection of the pure Pd on α-alumina sample with SEM confirmed the Pd layer to be 3–4 μm thick. Both the pure Pd and the Pd/Ag bi-sputtered sample were found to have dense metal layers with a smooth surface.

The XPS depth profile of the bi-sputtered sample showed a constant Ag content in the bulk of approximately 20 at%, but the surface showed a small Ag enrichment (25 at%). Thermodynamics[25,26] indeed dictate complete mixing of Pd and Ag in the bulk and Ag enrichment of the surface (caused by the lower surface energy of Ag). The homogeneity of the sample is thus as good as can be expected.

3.2 XANES and FEFF 8.2

In Fig. 2 the experimental XANES results are plotted. Fig. 2(a) exhibits the separate influences of dissolving hydrogen and alloying with Ag on the Pd L_3 edge XANES, whereas in Fig. 2(b) the Pd/Ag–H system is compared with the Pd–H system. The most prominent feature of the Pd vacuum XANES is the white-line at 3173 eV, caused by excitation of electrons from the 2p to the 4d band.[27] Although the atomic configuration of Pd is $4d^{10}5s^0$ hybridisation in the solid gives rise to

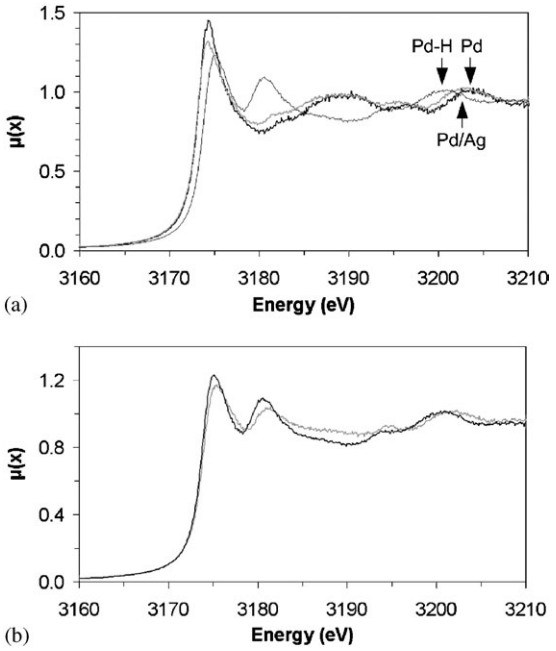

Fig. 2 Experimental results of (a) Pd in vacuum (black), Pd/Ag in vacuum (grey) and Pd in H_2 (thinner line), and (b) Pd in H_2 (black) and Pd/Ag in H_2 (grey).

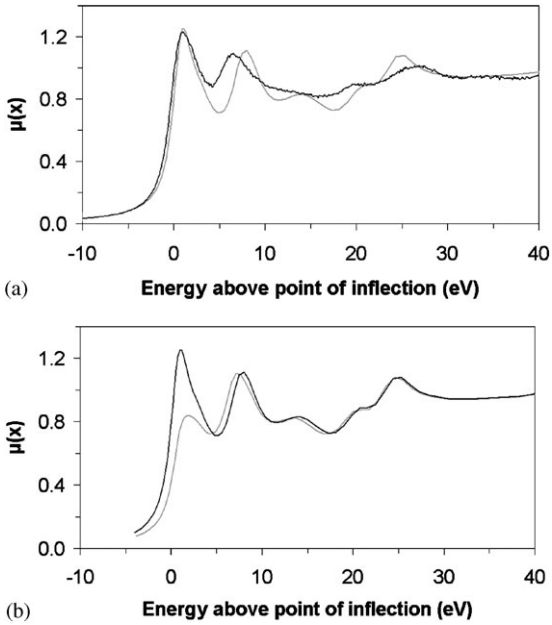

Fig. 3 Comparison of (a) Pd in H_2 exp. (black) and $PdH_{0.6}$, model #1 (grey), and (b) $PdH_{0.6}$, model #1(black) and $Pd_{0.8}Ag_{0.2}H_{0.6}$, model #2 (grey).

0.36 hole per atom in the 4d band as determined by Vuillemin and Priestly[28,29] using the de Haas van Alphen effect. This value was later confirmed by Mueller *et al.*[30] using *ab initio* calculations.

Fig. 2(a) shows that the addition of Ag to Pd gives a lower intensity of the white-line, which is in agreement with results in the literature.[16] This can be attributed to a decrease of the number of 4d holes in Pd, *i.e.*, to a shift of electron density from the Ag to the Pd metal. The peak at approximately 3204 eV (indicated with arrows) is shifted to lower energy for Pd/Ag. According to the $1/R^2$ rule[31] this indicates lattice expansion, in full agreement with the lattice constant data in the materials and methods section.

In addition, it can be concluded from Fig. 2(a) that dissolving hydrogen in Pd causes a similar shift in peak position of the 3204 eV peak (a stronger shift because of the larger lattice expansion) as well as a decrease in white-line intensity, a blue shift of the entire spectrum and a new feature at +7 eV from the white-line. This new peak has been attributed to the unfilled Pd 4d–H 1s anti-bonding orbital[13] formed due to the bonding of hydrogen. From here on this peak will be labelled "the hydrogen anti-bonding peak". The decrease of the white-line intensity, stronger than for the Ag case, is again caused by a decrease in the number of 4d holes as a result of a shift of electron density towards the Pd atoms. Finally, the blue shift is also a consequence of the strong shift in electron density. The energy required for the excitation of electrons from the 2p to the 4d band has increased due to the filling of the holes of lowest energy in the 4d band.

Fig. 2(b), seems to indicate that the Pd/Ag–H system is not a simple combination of the separate effects of Ag and H as described above. First of all, the decrease in white-line intensity between the two plots in Fig. 2(b) is smaller than the difference between Pd and Pd/Ag in Fig. 2(a). Secondly, the intensity of the hydrogen anti-bonding peak at 3181 eV has also significantly changed with respect to pure Pd.

The first FEFF results, Fig. 3(a), show that the Pd–H XANES is well reproduced with the $PdH_{0.6}$ model (#1) described in the materials and methods section. All experimental features are present with reasonable correct intensity and position, even the shoulder at 3194 eV is visible in the model results. This proves that the FEFF 8.2 program is suited to calculate the XANES of this kind of metal hydrides.

Application of the Pd–H model to the Pd/Ag–H system, by replacing 20% of the Pd atoms with Ag, did not result in a satisfactorily simulation of the experimental result. Fig. 3(b) shows that the intensity of the white-line of the $Pd_{0.8}Ag_{0.2}H_{0.6}$ model is much smaller than found experimentally (Fig. 2(b)). Furthermore, the FEFF calculations show the same intensity of the hydrogen anti-bonding peak for the Pd–H and Pd/Ag–H systems, while experimentally the peak is significantly weaker for the Pd/Ag–H system.

In the second Pd/Ag model (#3) the amount of dissolved hydrogen is, in line with the H_2 partial pressure/solubility relation at the experimental conditions,[32] reduced from 0.6 to 0.4 per metal atom. In Fig. 4 the calculated XANES of this model is plotted together with the $PdH_{0.6}$ model.

When this figure is compared with Fig. 2(b) it is clear that the experimental results are reproduced in great detail. Note that the Pd/Ag model result replicates the experimental decrease in white-line and hydrogen anti-bonding peak intensity. Though the amplitudes of the waves in the calculated spectra are stronger and the hydrogen anti-bonding peak is moved to slightly higher energy than found experimentally, all the experimental features are present and have correct relative intensities. Clearly the Pd/Ag–H XANES can be described as a combination of the separate effects of Ag and H described above and no other influences on the XANES have been detected. The large differences between Fig. 3(b) and Fig. 4 demonstrate the strong influence of the hydrogen content on the Pd/Ag–H XANES.

Fig. 5 demonstrates the influence of Ag clustering on the XANES. It can be seen that the intensity of the white-line of the Ag cluster model is significantly stronger compared to the evenly distributed Ag model. In our opinion this is a direct consequence of the fact that there are now fewer Ag atoms in close vicinity to the central Pd atom than in the evenly distributed model. This effect could be somewhat stronger experimentally since the XANES is an average of all Pd atoms and not just the ones adjacent to an Ag cluster. It is expected that Ag clustering will be observable with XANES, especially when the metals form sufficiently large pure Pd and pure Ag domains to influence the observed lattice constants. As

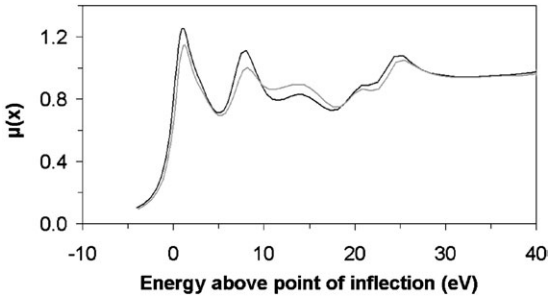

Fig. 4 Comparison of $PdH_{0.6}$, model #1 (black) and $Pd_{0.8}Ag_{0.2}H_{0.4}$, model #3 (grey).

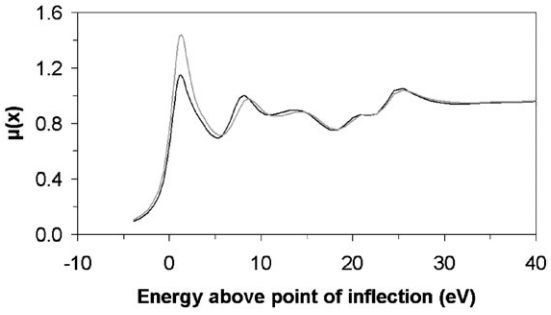

Fig. 5 Comparison of $Pd_{0.8}Ag_{0.2}H_{0.4}$ octahedral Ag randomly distributed, model #3 (black) and Ag clustered in one cube, model #4 (grey).

discussed for Fig. 2(a) lattice constant changes lead to shifts in peak positions.

4. Conclusions

For the first time the Pd/Ag–H XANES has been determined experimentally and modelled theoretically. A model of fcc-Pd/Ag with the Ag atoms evenly distributed through the system and the hydrogen atoms placed in the octahedral holes was able to explain the observed XANES in great detail. The Pd/Ag–H Pd L_3 edge XANES can be considered to be a combination of the separate effects of Ag and H on Pd.

The FEFF calculations show that the Pd/Ag–H system generates an anti-bonding Pd–H band, in close agreement with the experimental results. In addition the calculations show that the hydrogen content of the system strongly influences the XANES, especially the intensity of the white-line and the anti-bonding peak. In contrast the influence of the Ag atoms is limited to relatively small changes in the white-line intensity. However simulations showed that a change of the Ag distribution within the Pd/Ag fcc lattice from well-mixed to clustered has a significant influence on the Pd L_3 edge white-line intensity. The experiments show that, under the present conditions, the Pd/Ag–H system can be described as $Pd/AgH_{0.4}$ versus $PdH_{0.6}$ for the pure palladium system.

Acknowledgements

We thank Luci Correia of ECN for supplying the Pd sample, Hien Duy Tong of the MESA$^+$ Institute of Twente University for supplying the Pd/Ag sample and A. J. M. Mens of the U.U. for the XPS depth-profiling. The XANES work was supported by the IHP-Contract HPRI-CT-2001-00140 of the European Commission. The staff of HASYLAB beam line E4 (Kontantin Klementiev and Edmund Welter) is gratefully acknowledged. This research was carried out under a grant from NWO-CW (Netherlands Organization for Scientific Research, Chemical Sciences) with financial contributions of Shell Global Solutions International, Senter and the Dutch Ministry of Environmental Affairs. The research of FMFdG is supported by the Netherlands Research School Combination on Catalysis (NRSCC) and by a Science-Renewal Fund of NWO-CW. D. C. Koningsberger and D. Ramaker are acknowledged for valuable discussions.

References

1 S. Uemiya, *Sep. Purif. Methods*, 1999, **28**, 51.
2 S. Uemiya, T. Matsuda and E. Kikuchi, *J. Membrane Sci.*, 1991, **56**, 315.
3 S. N. Paglieri and J. D. Way, *Sep. Purif. Method.*, 2002, **31**, 1.
4 Y. S. Cheng and K. L. Yeung, *J. Membrane Sci.*, 1999, **158**, 127.
5 R. Dittmeyer, V. Höllein and K. Daub, *J. Mol. Catal. A*, 2001, **173**, 135.
6 S. Tosti, A. Basile, G. Chiappetta, C. Rizello and V. Violante, *Chem. Eng. J.*, 2003, **93**, 23.
7 J. N. Keuler and L. Lorenzen, *Ind. Eng. Chem. Res.*, 2002, **41**, 1960.
8 G. L. Holleck, *J. Phys. Chem.*, 1970, **74**, 503.
9 X. Ke and G. J. Kramer, *Phys. Rev. B*, 2002, **66**, 184304.
10 J. N. Keuler and L. Lorenzen, *J. Membrane Sci.*, 2002, **195**, 203.
11 A. G. Knapton, *Platinum Metals Rev.*, 1977, **21**, 44.
12 D. Fort, J. P. G. Farr and I. R. Harris, *J. Less-Common Met.*, 1975, **39**, 293.
13 A. V. Soldatov, S. D. Longa and A. Biancconi, *Solid State Commun.*, 1993, **85**, 863.
14 K. Ohtani, T. Fujikawa, T. Kubota, K. Asakura and Y. Iwasawa, *Jpn. J. Appl. Phys.*, 1998, **37**, 4134.
15 K. Kokko, R. Laithia, M. Alatalo, P. T. Salo, M. P. J. Punkkinen, I. J. Väyrynen, W. Hergert and D. Ködderitzsch, *Phys. Rev. B*, 1999, **60**, 4659.
16 I. Coulthard and T. K. Sham, *Phys. Rev. Lett.*, 1996, **77**, 4824.
17 I. A. Abrikosov, W. Olovsson and B. Johansson, *Phys. Rev. Lett.*, 2001, **87**, 1764031.
18 O. M. Løvvik and R. A. Olsen, *J. Alloy. Compd.*, 2002, **330–332**, 332.
19 L. C. Witjens, J. H. Bitter, A. J. van Dillen, F. M. F. de Groot, D. C. Koningsberger and K. P. de Jong, *Phys. Scr.*, 2004, accepted.
20 A. L. Ankudinov, B. Ravel, J. J. Rehr and S. D. Conradson, *Phys. Rev. B*, 1998, **58**, 7565.
21 S. L. M. Schroeder, G. D. Moggridge, R. M. Lambert, T. Rayment, in *Spectroscopy for Surface Science*, ed. R. J. H. Clark and R. E. Hester, Wiley, New York, 1998, ch. 1.
22 J. A. Bearden and A. F. Burr, *Rev. Mod. Phys.*, 1967, **39**, 125.
23 H. C. Jamieson, G. C. Weatherly and F. D. Manchester, *J. Less-Common Met.*, 1976, **50**, 85.
24 A. Ankudinov, B. Ravel, J. J. Rehr, *FEFF 8.00 Manual*, University of Washington: Seattle, 1999, p. 11.
25 I. Karakaya, W. T. Thompson, in *Binary Alloy Phase Diagrams*, 2nd edn., eds. T. B. Massalski, H. Okamoto, Metals Park: ASM International, 1991, vol. 3, p. 55–56.
26 O. L. J. Gijzeman, *Surf. Sci.*, 1985, **150**, 1.
27 T. K. Sham, *Phys. Rev. B*, 1985, **31**, 1888.
28 J. J. Vuillemin and M. G. Priestly, *Phys. Rev. Lett.*, 1965, **14**, 307.
29 J. J. Vuillemin, *Phys. Rev.*, 1966, **144**, 396.
30 F. M. Mueller, A. J. Freeman, J. O. Dimmock and A. M. Furdyna, *Phys. Rev. B*, 1970, **12**, 4617.
31 J. Stöhr, *NEXAFS Spectroscopy*, Springer Verlag, Berlin, 1992.
32 E. Wicke, H. Brodowsky, in *Topics in Applied Physics, Volume 29, Hydrogen in Metals II: Application-Oriented Properties*, eds. G. Alefeld, J. Völkl, Springer-Verlag, Berlin, 1978, Chapter 3, p. 118.
33 S. D. Axelrod and A. C. Makrides, *J. Phys. Chem.*, 1964, **68**, 2154.
34 P. Eckerlin, H. Kandler, in *Landolt-Börnstein, Numerical Data and Functional Relationships in Science and Technology, Group III: Crystal and Solid State Physics*, ed. K.-H. Hellwege, Springer-Verlag, Berlin, 1971, vol. 6, p. 202.

